# Improved Wake-Up Receiver Architectures with Carrier Sense Capabilities for Low-Power Wireless Communication

Robert Fromm, Lydia Schott and Faouzi Derbel

## Abstract

For power-limited wireless sensor networks, energy efficiency is a critical concern. Receiving packages is proven to be one of the most power-consuming tasks in a WSN. To address this problem, the asynchronous communication is based on wake-up receivers. The proposed receiver circuit can detect on-off keying pulses inside the 868 MHz band with a sensitivity of –60 dBm. The power consumption of the circuit is only 3.6 µW. The circuit design is kept simple, only requiring commercial off-the-shelf components like general-purpose operational amplifiers and comparators.

## Keywords

Wake-up receiver (WuRx), Wireless sensor network (WSN), Ultra-low power (ULP), Collision avoidance, Carrier sensing, Energy detection, LF correlation, Passive RF architecture, Operational amplifier, Comparator, Schottky diode, Envelope detector.

## 1 Introduction

The use of wireless sensor networks (WSNs) in research and industry is steadily increasing. WSNs are essential for the sensing and collection of environmental data in different application fields [CK03]. Powering sensor nodes using small batteries is often mandatory. Recharging and swapping batteries is usually not possible or would lead to higher maintenance costs. Parameters like latency, transmission range, and sensitivity are likewise major parameters when designing the hardware of a sensor node.

A continuous or a real-time wireless communication is nowadays essential for many applications when building an autonomous WSN. To maintain such a wireless communication even with modern wireless transceivers would lead to a power consumption greater than 10 mW. In order to power such a sensor node for a long period with a battery, the receiving and sending intervals need to decrease significantly. This inevitably leads to increased latency and response times of the WSN.

A wake-up receiver (WuRx) is a special RF receiver that enables the sensor node to be in a continuous receiving mode. Different approaches with passive and active components exist in order to keep the WuRx's power consumption below 10 µW. Figure 1 shows how a WuRx can be integrated into a sensor node.
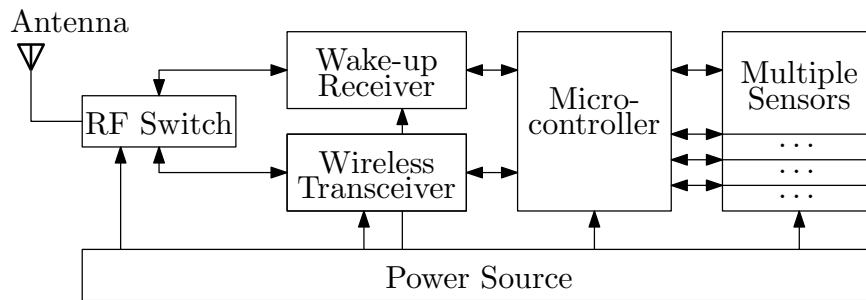


Figure 1: A wireless sensor node with a WuRx based on [Gam+10]. A RF switch is used to separate both receiving paths of WuRx and wireless transceiver.

A sensor node is typically built out of antenna, wireless transceiver, sensors, energy source, and microcontroller. Due to the WuRx, a second RF reception path is introduced. Either the wireless transceiver receives data packets or the WuRx receives wake-up packets (WuPts). Multiple antennas can be used or an RF switch is introduced in order to switch between these two RF paths. The microcontroller takes care of the configuration of the WuRx. During standby, the WuRx is typically the only active component in the circuit. If a WuPt is received, the WuRx sends an interrupt to the microcontroller to wake up. [Gam+10].

The WuRx implementations are divided into two categories: application-specific integrated circuit (ASIC)-based WuRx and WuRx implemented using commercial off-the-shelf (COTS) components [Piy+17]. This paper will focus on the COTS implementations of WuRx, because of a much better repeatability of results, simpler, and cheaper implementations and integration of a WuRx in a commercial product. In Figure 2 the typical building blocks of a COTS WuRx can be seen.

The WuRx's input signal is characterized with low amplitude, high noise figure, and various interferences. Usually, an RF band-pass filter is used to pass only signals of the desired frequency bands. A passive envelope detector performs the signal detection and conversion to a LF signal. An impedance matching circuit is
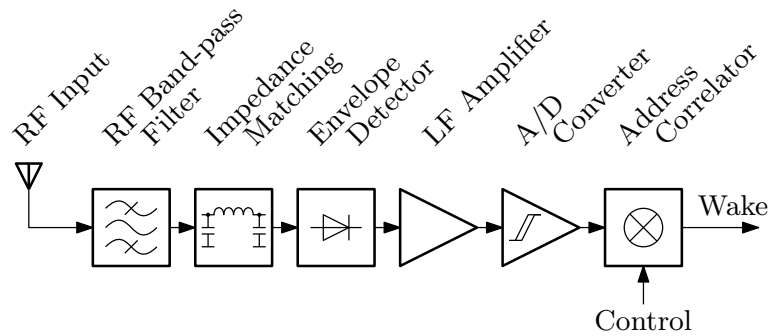
Figure 2: Building blocks of a typical COTS WuRx with passive envelope detector

needed to avoid power losses through signal reflection from the envelope detector. The LF amplifier circuit is needed to boost the rectified signal to be detectable by the following analog-to-digital converter circuit. A digital address correlator can be added to implement addressing capabilities of the WuRx and avoid false wake-ups [FSD21].

# 2 Related Work

One of the first COTS implementations is [APM08]. This implementation uses a passive RF front end. A single comparator with a fixed reference voltage is used as the only active component in the circuit. The mentioned power consumption of 2.6 μW is interesting, but the sensitivity of the circuit can be expected as very low. The given maximum range is 10 m when using 868 MHz as the carrier frequency. The implementation of [Mag+16] improves the previous implementation by introducing an adaptive threshold, adding further measurements and investigations. The performance of three different COTS comparators were investigated. The maximum sensitivity of −55 dBm was achieved with the LPV7215 with a power consumption of 1.2 μW. With comparator TLV3691, only −32 dBm and 152 nW were achieved.

Our implementation [FSD21] added a base-band amplifier using COTS operational amplifiers (OAs). Signals up to −50 dBm can be detected reliably, but the power consumption increased to 4.2 μW. Further investigations were made, in order to use the circuit for both transmitter and receiver power savings.

[Kaz+21] proposes a design with OA and comparator, that claims to reach a sensitivity of −70 dBm with a power consumption below 1 μW. This is possible due to a very slow data rate of approximately 20 bit/s, resulting in a huge power consumption of the wake-up transmitter (WuTx).

A different approach for implementing a WuRx lies in using a special integrated circuit acting as a LF WuRx. One of the first implementations is [Gam+10] us-

ing the AS3932. A specially modulated WuPt needs to be sent in order to fulfill the AS3932 packet requirements. The proposed WuRx reaches a sensitivity of −52 dBm and an idle power consumption of approximately 8.3 µW.

[BDK18b] improved these designs further by using an AS3933 and adding a power-gated LF amplifier circuit. The power-gating is controlled by a OA and comparator circuit. The power consumption of the circuit is approximately 7.3 µW and the sensitivity increased to −61 dBm. Recent publications using the AS3933 like [CAM20; GS+20] could not reduce the power consumption nor improve the sensitivity.

The WuRx's sensitivity is limited due to the noise level of the passive diode detector circuit. Overcoming this limit, the implementation of [BDK18a] added a duty-cycled low-noise amplifier (LNA) resulting in a sensitivity of −90 dBm. During active phase, the power consumption reaches over 1 mW. Through duty-cycling an average power consumption of only 3 µW. Because of duty-cycling, the latency increases to 30 ms.

# 3 Theoretical Analysis

The different building blocks of a COTS WuRx are shown in Figure 2. The following subsections describe and analyze them theoretically.

## 3.1 Envelope Detector's Diode Calculation

All the implementations [APM08; BDK18a; BDK18b; CAM20; FSD21; GS+20; Gam+10; Kaz+21; Mag+16] are using enveloped detectors with zero-biased Schottky diodes. Using diode based envelope detectors is one of the ways to passively demodulate an RF signal. While active mixer circuits are capable of demodulating multiple modulation types, envelope detector can only be used for amplitude-modulated signals, e. g. on-off keying (OOK) . The envelope detector consists of a non-linear element performing a rectification process. After low-pass filtering, only the LF parts of the signal remain.

The diode's open-circuit output voltage $V_{\text{out}}^{\text{OC}}$ can be modeled as a function of the incident RF power $P_{\text{in}}$. This function can be divided into two regions. A linear region for larger input powers with $P_{\text{in}}$ proportional to $V_{\text{out}}^{\text{OC2}}$ and the square-law region for smaller input powers with $P_{\text{in}}$ proportional to $V_{\text{out}}^{\text{OC}}$. The limit of the square-law region can be seen in Equation 1, with $V_{\text{T}}$ the thermal voltage and $n$

the diode's ideality factor [BB03, p. 585].

$$V_{\text{out}}^{\text{OC}} < nV_{\text{T}} \approx 26\,\text{mV}, \quad \text{with } n \approx 1, T = 300\,\text{K} \tag{1}$$

Because of low input powers in WuRx applications, the following analyses will be focused on the square-law region of the diode. Equation 2 is the definition of the open-circuit voltage sensitivity $\gamma^{\text{OC}}$ [BB03, p. 568].

$$V_{\text{out}}^{\text{OC}} = \gamma^{\text{OC}} \cdot P_{\text{in}} \tag{2}$$

The diodes behavior can be modeled as a Thévenin equivalent, with the open-circuit voltage $V_{\text{out}}^{\text{OC}}$. The equivalent resistance is often called video resistance $R_{\text{v}}$. $R_{\text{v}}$ is defined by the diode's series resistance $R_{\text{s}}$ and the diode's junction resistance $R_{\text{j}}$, see Equation 3 [BB03, p. 569].

$$R_{\text{v}} = R_{\text{s}} + R_{\text{j}} \tag{3}$$

Equation 4 is the formula of the diode's junction resistance, with $I_{\text{s}}$ the diode's saturation current and bias current $I_{\text{DC}}$. $I_{\text{DC}} = 0$ for a zero-biased envelope detector [BB03, p. 566].

$$R_{\text{j}} = \frac{nV_{\text{T}}}{I_{\text{s}} + I_{\text{DC}}} \tag{4}$$

The open-circuit voltage sensitivity is calculated by Equation 5 with $C_{\text{j}}$ the diode's junction capacitance and $\omega_{\text{carr}} = 2\pi f_{\text{carr}}$ the RF carrier frequency [BB03, p. 574].

$$\gamma^{\text{OC}} = \frac{1}{2nV_{\text{T}}} \cdot \frac{R_{\text{j}}}{1 + \rho(1 + v^2)}, \quad \text{with } \rho = \frac{R_{\text{s}}}{R_{\text{j}}}, v = \omega_{\text{carr}} C_{\text{j}} R_{\text{j}} \tag{5}$$

The sensitivity of the diode for envelope detection is not only dependent on the voltage sensitivity, but also affected by the diode's noise figure. The diode's noise voltage is defined by the Johnson-Nyquist noise through the video resistance $R_{\text{v}}$. The Equation 6 shows the calculation with $k_{\text{B}}$ the Boltzmann constant and $f_{\text{B}}$ the LF-signal bandwidth [BB03, p. 570].

$$V_{\text{n}} = \sqrt{4k_{\text{B}}Tf_{\text{B}}R_{\text{v}}} \tag{6}$$

The tangential signal sensitivity (TSS) $P_{\text{TSS}}$ is defined as the minimum RF power level, where the LF signal's amplitude is larger than the noise peak-to-peak value.

The relationship of $V_{\mathrm{out}}^{\mathrm{OC}} = 2.8 \cdot V_{\mathrm{n}}$ is used [BB03, pp. 570f].

$$P_{\mathrm{TSS}} = \frac{2.8 \cdot \sqrt{4k_{\mathrm{B}}Tf_{\mathrm{B}}R_{\mathrm{v}}}}{\gamma^{\mathrm{OC}}} \tag{7}$$

The diode HSMS-2852 from Agilent Technologies is the typical diode used in the envelope detector by many publications [APM08; BDK18b; GS+20; Kaz+21; Mag+16]. Because this diode is not any more provided by the manufacturer, an alternative is needed. The SMS7630-006LF from Skyworks Solution Inc. has nearly identical parameters and the following investigations were made, to ensure that the diode SMS7630 is a good alternative diode [FSD21]. A theoretical analysis of the parameters defined in the previous equations was made. Table 1 shows the results.

Table 1: Comparison of HSMS-2852 and SMS7630 - calculated parameters [Agi05; Sky18]

| Parameter | HSMS-2852 | SMS7630 |
|---|---:|---:|
| $n$ | 1.06 | 1.05 |
| $R_{\mathrm{s}}$ | 25 Ω | 20 Ω |
| $C_{\mathrm{j}}$ | 180 fF | 140 fF |
| $I_{\mathrm{s}}$ | 3 µA | 5 µA |
| $nV_{\mathrm{t}}$ | 27.4 mV | 27.1 mV |
| $R_{\mathrm{j}}$ | 9.13 kΩ | 5.43 kΩ |
| $R_{\mathrm{v}}$ | 9.16 kΩ | 5.45 kΩ |
| $\gamma^{\mathrm{OC}}$ | 162 mV/µW | 98.1 mV/µW |
| $P_{\mathrm{TSS}}$ | –76.7 dBm | –75.7 dBm |

$$T = 300\,\mathrm{K}, f_{\mathrm{carr}} = 868\,\mathrm{MHz}, f_{\mathrm{B}} = 10\,\mathrm{kHz}$$

The small parameters deviations result into slightly different values for $R_{\mathrm{j}}$, $R_{\mathrm{v}}$, and $\gamma^{\mathrm{OC}}$. But the values for the TSS are nearly identical, resulting in an nearly equal performance of both diode types.

## 3.2 Envelope Detector Architecture

When designing an envelope detector, single or multiple diodes in different configurations can be used. Such diode rectifiers are typically used in RF energy harvesting applications [TCP17]. It shall be noticed, that WuRx applications are faced to much lower RF input powers. Figure 3 shows a selection of the implementations utilized in WuRxs. Earlier implementations like [APM08] are utilizing a Dickson voltage multiplier and most of the current implementations like [BDK18a; BDK18b; CAM20; FSD21; GS+20; Gam+10; Kaz+21; Mag+16] use the

Greinacher voltage doubler. The performance of a single-diode implementation shall be investigated.



(a) Single diode    (b) Greinacher voltage doubler


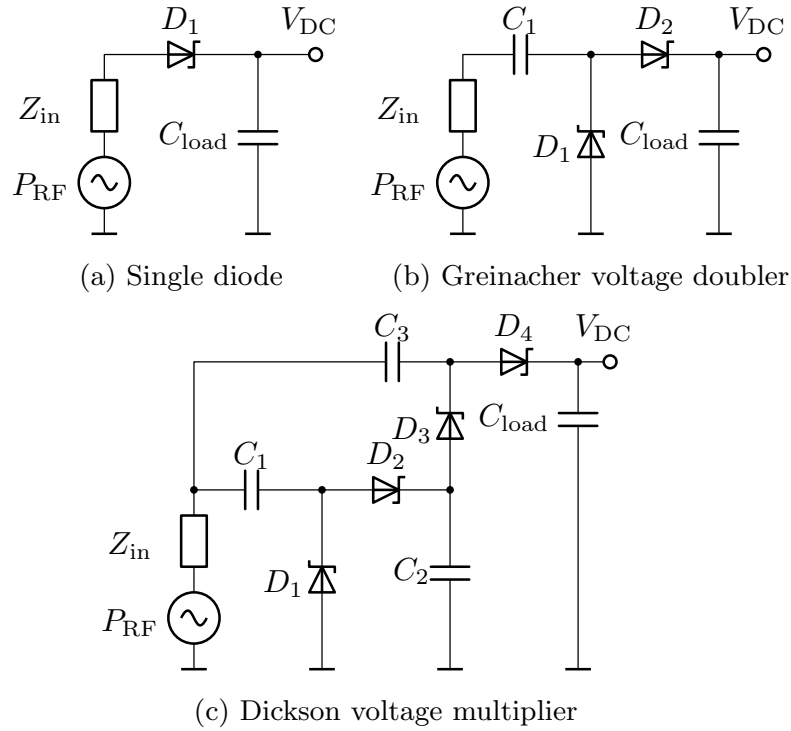
(c) Dickson voltage multiplier

Figure 3: A selection of envelope detector architectures utilized in WuRxs

The performance of the single diode (SD) and voltage doubler (VD) circuit will be investigated through measurements. The performance of the corresponding architecture is highly dependent on the utilized impedance matching network. Because the diodes' impedance is typically not equal to the previous building block's output impedance, most of the signal power is reflected, resulting in a lower diode's output voltage.

## 3.3 Impedance Matching Circuit

Many impedance matching circuits for diode rectifier were investigated in the context of RF energy harvesting. Typically either strip lines or lumped components are used [TCP17]. The selection of WuRx implementations [APM08; BDK18a; BDK18b; CAM20; FSD21; GS+20; Gam+10; Kaz+21; Mag+16] are utilizing an L-shaped network with one inductor and one capacitor. Figure 4 shows the resulting RF circuit when utilizing a VD.

The RF band-filter is modeled as $C_1$. The L-shaped LC matching is represented through the components $C_2$ and $L_1$. In order to fulfill a full-wave rectification for the Greinacher voltage doubler, $C_3$ is needed as a coupling capacitor. $C_4$ acts as a low-pass filter to remove the remaining RF components.
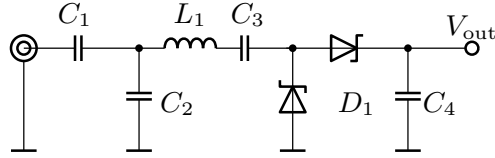
Figure 4: WuRx's RF circuit with VD. RF band-pass filter is modeled as capacitor $C_1$.

When utilizing a SD, the capacitor $C_1$ interrupts the DC return path of the circuit. This results into a rather low and distorted voltage output of the enveloped detector. An RF choke [Sky08] or an impedance matching circuit with two inductors can be utilized. Figure 5 shows the resulting schematic.
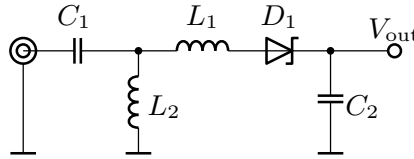


Figure 5: WuRx's RF circuit with SD. RF band-pass filter is modeled as capacitor $C_1$.

## 3.4 RF Band-pass Filter

An envelope detector matched to the precise center frequency is susceptible to RF signals from different frequency bands. To avoid such interferences, an RF band-pass filter of the desired frequency band shall be introduced. Surface acoustic wave (SAW) filters allowing only a narrow-band transmission are available as COTS parts. Because of the insertion loss of the SAW filter, the output voltage of the envelope detector is reduced.

The utilized SAW filter B39871B3725U410 has a center frequency of 869 MHz, a bandwidth of 2 MHz, and a typical insertion loss of 2.5 dB [RF319]. Because of the envelope detector's square-law behavior, this leads to a reduction of the output voltage of 44 %. The decrease of the WuRx's sensitivity is equal to the filter's insertion loss, but the utilization of a SAW filter in a noisy real-live environment is essential.

## 3.5 LF Amplifier

The envelope detector's voltage output needs to be amplified in order to be detectable by the following A/D converter. Operational amplifiers (OAs) are used as voltage amplifiers in implementations like [BDK18b; FSD21; Kaz+21]. [BDK18a] introduces a voltage amplifier with two bipolar junction transistors (BJTs).

### 3.5.1 Gain-Bandwidth Product

Supply current and gain bandwidth product (GBWP) are highly dependent on each other. Amplifiers with high GBWP are allowing high amplification factors while maintaining fast response time and high data rates. Figure 6 shows the GBWP and supply current of a selection of suitable COTS OAs. The implementation of [BDK18b] used ISL28194, [FSD21] used TLV512, and [Kaz+21] used LPV611.
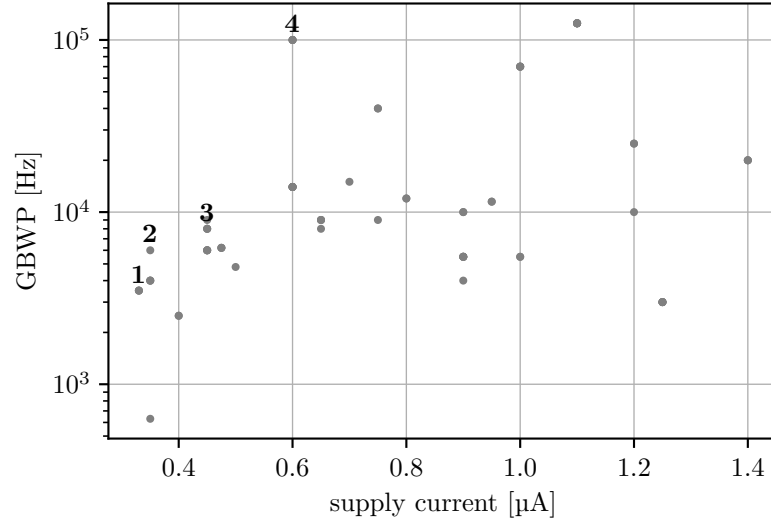


Figure 6: GBWP and supply current of selection of operational amplifiers. Marked devices: 1) ISL28194, 2) TLV512, 3) LPV611, 4) MCP6141

When choosing the right OA for the circuit, a trade-off between current consumption and reaction time has to be made. A lower current consumption means a lower GBWP. A low GBWP leads to a slow reaction time because of a slower settling time of the OAs. To convert the GBWP to the settling time $t_{settle}$ the Equation 8 can be used as an approximation. In Equation 8 $\tau$ represents the time constant, $\omega_k$ the angular low-pass filter cut-off frequency, $f_k$ the cut-off frequency, and $A_F$ the voltage amplification factor [FSD21].

$$t_{settle} \approx 3\tau = \frac{3}{\omega_k} = \frac{3}{2\pi \cdot f_k} = \frac{3 \cdot A_F}{2\pi \cdot GBWP} \tag{8}$$

### 3.5.2 Operational Amplifier Circuit Design

In order to meet the power delivery restraints of a WSN, only a single-rail supply can be used for the amplifier circuitry. When designing an amplifier, the input and output signals must match the input and output voltage swings of the OA. Figure 7 shows inverting and non-inverting amplifier circuits with corresponding
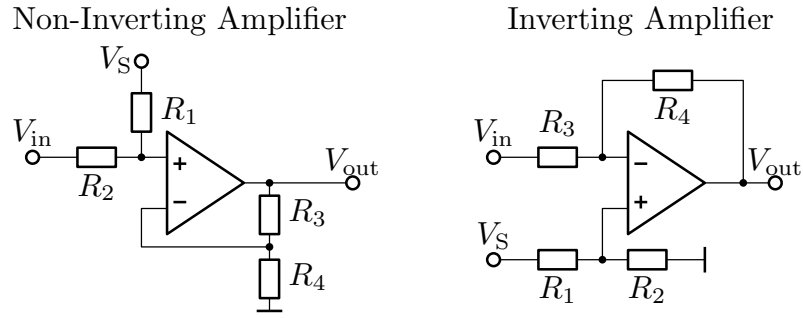
biasing circuits [Tex01].



Figure 7: Non-inverting amplifier with biasing circuit and inverting amplifier with reference voltage generator.

When utilizing an inverting amplifier, a reference voltage source needs to be introduced. This is shown in Figure 7 by the voltage divider $R_1$ and $R_2$. Adding a biasing circuit to a non-inverting amplifier is necessary to overcome possible input voltage offsets.

Ultra-low-power OAs typically have a rather high input voltage offset. For instance, the TLV512 has a typical offset voltage of $\pm100\,\mu V$ and $\pm3\,mV$ at temperature extremes. With an envelope detector voltage sensitivity of $\gamma = 40\,mV/\mu W$, signal level of only $-56\,dBm$ or $-41\,dBm$ can be detected accordingly. Both biasing circuit and reference voltage generator will increase the power consumption defined by the supply voltage $V_S$ and both resistor values $R_1, R_2$.

### 3.5.3 BJJT based amplifiers

Previous simulations and experiments showed, that it is possible to use RF BJTs like the BFP405 as a low-power LF amplifier. Using an ultra low-current biasing circuit promising higher GBWPs and lower supply currents than OA circuits. A combination of a common-emitter and common-collector configuration is used because of its high voltage gain, high input impedance, and low output impedance. Figure 8 shows amplifier circuit
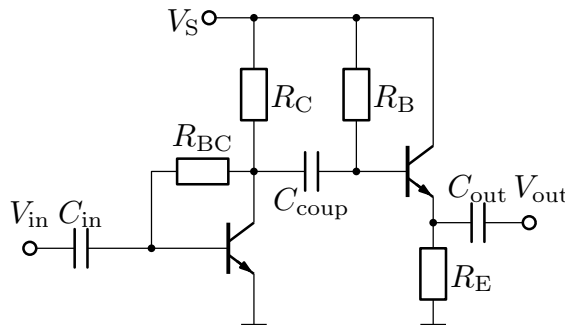


Figure 8: Common-emitter and common-collector stage of a BJT based amplifier

Simulations were used to optimize the component values according to the desired frequency response, gain, and current consumption. With $C_{in} = C_{coup} = C_{out} = 1\,\text{nF}$, $R_{BC} = R_B = 100\,\text{M}\Omega$, $R_C = 10\,\text{M}\Omega$, and $R_E = 5\,\text{M}\Omega$ a gain of 43 in the range of 500 Hz to 10 kHz was reached. The circuit's current consumption is around 530 nA.

## 3.6 Comparator Circuit

To make the analog output signal of the LF amplifier detectable to the digital address decoder, an analog-to-digital converter is utilized. The implementations [APM08; BDK18a; FSD21; Kaz+21; Mag+16] are utilizing comparator as 1 bit converters.

### 3.6.1 Input Offset Voltage

[Mag+16] compared the performance of the TLV3691, AS1976, and LPV7215 and stated that input offset voltage is the comparator's sensitivity-limiting factor. Many low-power comparators have a built-in input hysteresis, which is often higher than the typical input offset figure. The hysteresis is the minimum voltage difference on the comparator that needs to be overcome in order to latch the compactor output. Table 2 shows the performance of three low-power comparator circuits. TS880 was added because AS1976 is no longer COTS available. The minimum detectable signal (MDS) is the sum of input offset and hysteresis. The last row shows the theoretical WuRx's sensitivity if the comparator circuit is connected directly to the envelope detector.

Table 2: Comparison of multiple COTS comparators [Tex15; ams07; STM13; Tex16a]

| Parameter | TLV3691 | AS1976 | TS880 | LPV7215 |
|---|---|---|---|---|
| Supply current (typ.) [nA] | 75 | 200 | 300 | 790 |
| Propagation delay (typ.) [µs] | 45 | 15 | 7 | 13 |
| Input offset (typ.) [mV] | 3 | 1 | 1 | 0.3 |
| Input offset (max.)[1] [mV] | 17 | 5 | 10 | 6 |
| Hysteresis [mV] | 17 | 3 | 2.6 | 0 |
| MDS[2] [mV] | 34 | 8 | 12.6 | 6 |
| Sensitivity[3] [dBm] | −30.7 | −37.0 | −35.0 | −38.2 |

[1] $T = 25\,°\text{C}$, [2] minimum detectable signal, [3] with $\gamma = 40\,\text{mV}/\mu\text{W}$

The sensitivity value of −55 dBm stated by [Mag+16] can only be reached if comparator's typical input offset applies. Input offset distribution charts like [Tex15, Figure 21] show that the typical value only applies in a small proportion of the

manufactured circuits. This makes the utilization of such a comparator in a commercial product unfeasible. The utilization of a LF amplifier circuit is inevitable.

### 3.6.2 Reference Generator

The implementations [APM08; BDK18b; FSD21] are using a comparator with a constant reference voltage, typically generated by a voltage divider. [BDK18a; Kaz+21; Mag+16] are using an adaptive reference voltage generated by an *RC* circuit. Figure 9 shows the schematic of both implementations.
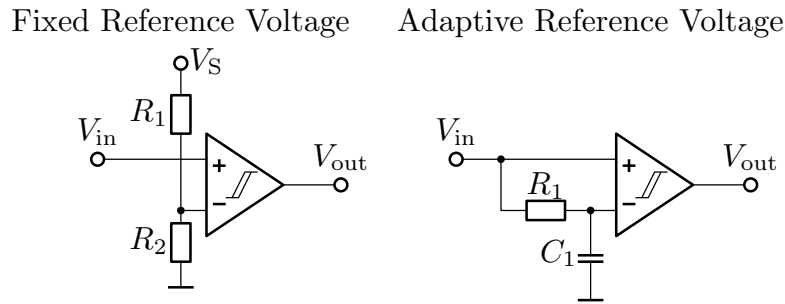


Figure 9: Fixed and adaptive reference generator for comparator circuit

Using a fixed reference voltage leads to additional power consumption. While the fixed reference voltage's turn-on time is near zero, the adaptive reference voltage takes several milliseconds in order to charge $C_1$ to the correct voltage level. The adaptive reference level makes it easier to detect periodic square-wave signals, because the reference voltage is charged up to half of the signal amplitude. Fixed reference voltage makes it easier to detect single impulses in case of a carrier sensing implementation.

# 4 Experimental Analysis

## 4.1 Impedance Matching

Four different test printed circuit boards (PCBs) were built-up in order to investigate the envelope detector behavior. Table 3 shows the configuration of these PCBs, with [1] being the reference PCB, [2] utilizing the HSMS2852 diode, [3] utilizing the single diode (SD) configuration, and [4] with the SAW filter added. The components' values of the impedance matching network was derived from the simulation. Small adjustments were made in order to overcome additional parasities and set the center frequency as close as possible to 868 MHz. PCB [4] needed to be matching before the SAW filter was added. Figure 10 shows the reflection factor of PCB [1] and [4].

Table 3: Configuration of the envelope detector test PCBs

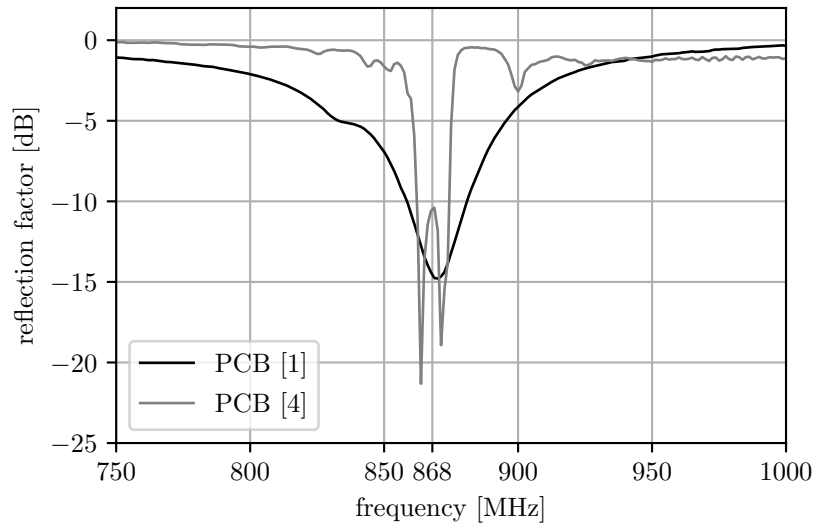| PCB | Diode | Diode Configuration | SAW filter |
|-----|-------|---------------------|------------|
| [1] | SMS7630-006LF | VD | no |
| [2] | HSMS2852 | VD | no |
| [3] | SMS7630-079LF | SD | no |
| [4] | SMS7630-006LF | VD | B39871B3725U410 |



Figure 10: Reflection factor of test PCB with [1] and without the SAW filter [2]

The reached reflection factor on PCB [1] is approximately $\Gamma_{[1]} = -15\,\text{dB}$. The SAW filter creates a more narrow-band matching. The minimum refection factor is approximately $\Gamma_{[4]} = -10\,\text{dB}$.

## 4.2 Envelope Detector

### 4.2.1 Voltage Sensitivity

With the following experiment the voltage sensitivity of four different envelope detector configurations (see Table 3) was measured. Figure 11 shows the block diagram of the measurement setup. The signal generator produced an OOK signal with a low frequency of 1 kHz. The power and carrier frequency of the signal generator can be varied. In order to make the small signal levels detectable by the oscilloscope, a differential LNA was added. The oscilloscope is measuring the signal amplitude due to a 1 kHz OOK-modulated signal. Figure 12 shows the envelope voltage of PCB [1] at an input level of −50 dBm. The measured signal amplitude is around 450 μV. The oscilloscope images of the other PCBs were nearly identical.
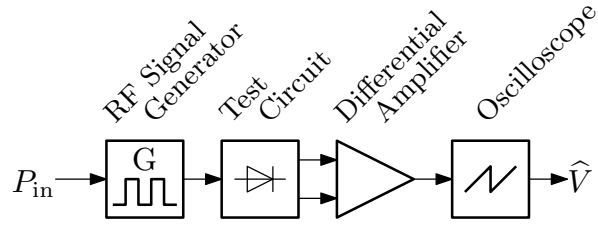
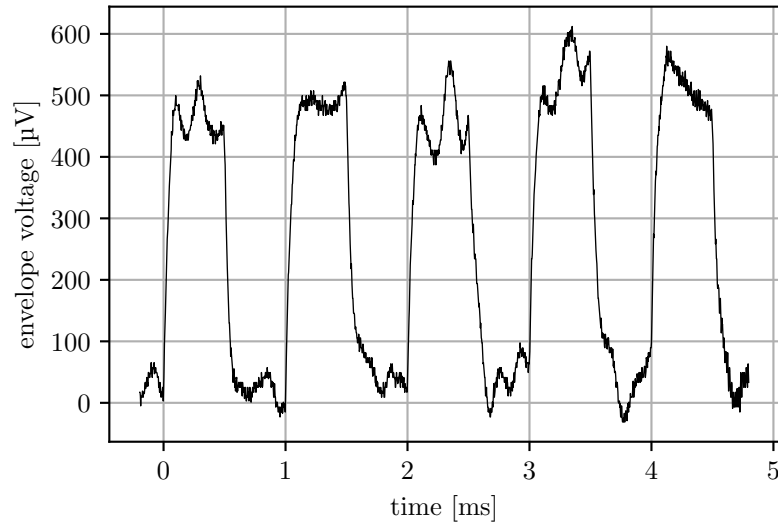Figure 11: Block diagram of the voltage sensitivity measurement



Figure 12: Envelope voltage of PCB [1] at an input level −50 dBm

Figure 13 shows the envelope voltage of each PCBs at multiple input power levels. The figure shows clearly the square-law behavior of the envelope detector for input levels lower −30 dBm and the linear behavior for input levels higher −20 dBm. The voltage sensitivity was averaged over the square-law region. PCB [1] resulted into $\gamma_{[1]} = 45\,mV/\mu W$, PCB [2] $\gamma_{[2]} = 58\,mV/\mu W$, PCB [3] $\gamma_{[3]} = 28\,mV/\mu W$, and PCB [4] $\gamma_{[4]} = 22\,mV/\mu W$.

The calculated voltage sensitivity values could not be reached due to additional losses and mismatches. As calculated, the voltage sensitivity of the HSMS2852 is slightly higher than the SMS7630's. Using the SD configuration instead of a VD results into a lower input voltage even at low input levels. Adding the SAW filter halves the output voltage, due to an insertion loss of nearly 3 dB.

### 4.2.2 Video Resistance

Verifying and measuring the value of video resistance $R_v$ is important to make sure, that the amplifier's input impedance does not lower the envelope voltage. The video resistance is the internal resistance of the Thévenin equivalent. Equation 9 shows the calculation of the video resistance, when measuring the open-
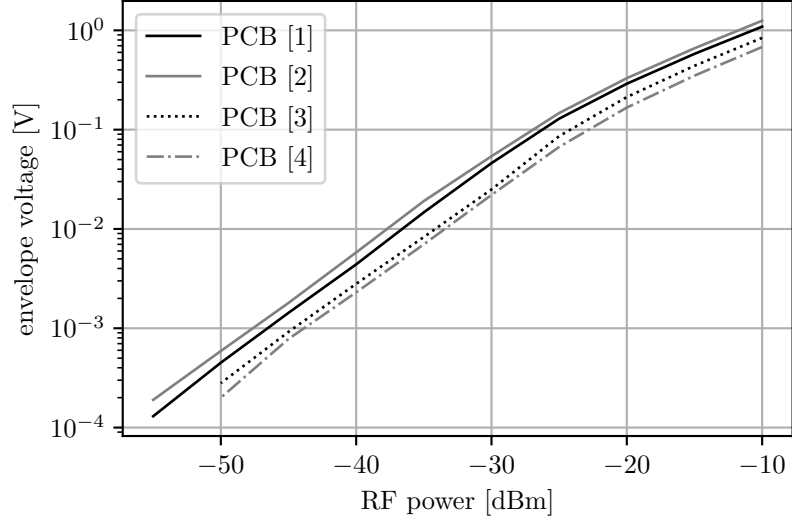
14

Figure 13: Measurement of the voltage sensitivity of four test PCBs

circuit envelope voltage $V_{out}^{OC}$ and the output voltage $V_{out}$ with an additional load resistance $R_L$.

$$R_v = R_L \cdot \left( \frac{V_{out}^{OC}}{V_{out}} - 1 \right) \tag{9}$$

Table 4 shows the measurements and resulting video resistance. The measurements were made with an RF power of −30 dBm to ensure proper square-law region behavior. The calculated video resistance $R_{v,calc.}$ is derived from Table 1. The video resistance needs to be doubled when using the using a VD configuration.

Table 4: Measurements and calculations of the video resistance of the four test configurations

| PCB | $V_{out}^{OC}$ [mV] | $R_L$ [kΩ] | $V_{out}$ [mV] | $R_{v,meas.}$ [kΩ] | $R_{v,calc.}$ [kΩ] |
|---|---|---|---|---|---|
| [1] | 47.1 | 10 | 21.7 | 11.7 | 10.9 |
| [2] | 60.7 | 10 | 25.7 | 13.6 | 18.3 |
| [3] | 29.3 | 10 | 16.9 | 7.3 | 5.45 |
| [4] | 23.6 | 10 | 11.1 | 11.2 | 10.9 |

The comparison of the measured and calculated video resistances shows, that the measurements of PCBs [1] and [4] are a good match. The video resistance measurement of the PCB [3] utilizing the SD configuration is slightly too high. The measurement of PCB [2] utilizing the HSMS2852 diode is significantly to low. A video resistance of around 11 kΩ can be estimated for the configurations of PCB [1] and [4].

## 4.3 Comparator Performance Test

Based on the following experiment, the performance of different comparator circuits will be evaluated. The comparators TLV3691, TS881, and LPV7215 will be utilized and compared following the selection of [Mag+16]. Because the AS7619 is no longer available, the TS881 was introduced due to its similar specifications. Figure 14 shows the utilized schematic of the test PCB. The RF front-end configuration [4] was used. The components $R_1$ and $C_3$ are forming the adaptive comparator threshold.
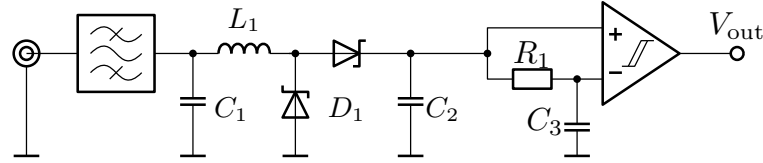


Figure 14: Schematic of the comparator test PCBs with RF front-end according to PCB [4], comparator with adaptive threshold

An 868 MHz RF signal with a 5 ms pulse every 100 ms was used to test the three comparators. Values of 1 MΩ and 10 nF were used for $R_1$ and $C_3$ accordingly. Both the RF front-end output and the comparator output were measured by an oscilloscope. This way the minimum signal amplitude, minimum RF level, and propagation delay can be measured. Table 5 shows the measurements results.

Table 5: Measurement results of comparator performance test

| Parameter | TLV3691 | TS881 | LPV7215 |
|---|---|---|---|
| Calculated MDS[1,2] [mV] | 34 | 12.6 | 6 |
| Calculated sensitivity[2] [dBm] | −30.7 | −35.0 | −38.2 |
| Propagation delay (typ.) [µs] | 45 | 7 | 13 |
| MDS[1] [mV] | 21 | 4.5 | 0.54 |
| Minimum RF level [dBm] | -31 | -38 | -47 |
| Propagation delay [µs] | 80 | 8 | 28 |

[1] minimum detectable signal, [2] see Table 2

The TLV3691 circuit detected a signal of −31 dBm and the TS881 of −38 dBm. These results are quite similar to the calculated from Table 2. For smaller signals, the comparator output stayed at a constant signal level. The comparator's hysteresis prevents unwanted signal changes through interferences or noise.
The test circuit utilizing the LPV7215 was able to detect a signal down to −47 dBm. Because LPV7215 has no internal hysteresis, the input offset voltage is the only limiting factor. This leads to interferences triggering the comparator output if a low input signal is present.

## 4.4 LF Amplifier Test

The following experiments are used to investigate the performance of amplifier circuits in detail. Three different amplifiers were built up and their performance is measured. The first two are OA-based designs. Amplifier [1] is utilizing the ultra-low-power TLV521 [Tex16b]. Amplifier [2] is utilizing the non-unity-gain-stable OA MCP6141 with a very high GBWP and a low power consumption [Mic19]. Amplifier [3] is built up using two transistors BFP405 in a common-emitter and common-collector configuration. Table 6 summarizes the most important specifications of these three designs.

Table 6: LF amplifier test circuits [Tex16b; Mic19]

| Parameter | [1] | [2] | [3] |
|---|---|---|---|
| Amplifier type | OA-based | OA-based | BJT-based |
| OA / BJT | TLV521 | MCP6141 | BFP40 |
|    Current consumption (typ.) | 350 nA | 600 nA | — |
|    GBWP (typ.) | 6 kHz | 100 kHz | — |
|    Input offset (max.) | 3 mV | 3 mV | — |
| Gain setting | ×200 | ×30 | — |
| Bandwidth (calc.) | 30 Hz | 3.3 kHz | — |
| Biasing current consumption | 300 nA | 300 nA | 530 nA |
| Total current consumption | 650 nA | 900 nA | 530 nA |

All three designs were built up. To verify the frequency behavior of the amplifier circuits the gain was measured in the range of 10 Hz to 20 kHz. Figure 15 shows the frequency response of the three amplifier circuits.

As expected, the first two amplifier circuits have a low-pass filter's frequency response. Amplifier [1] has a very low cut-off frequency. The cut-off frequency of amplifier [2] is around 1 kHz. Amplifier [3] has a band-pass filter's frequency response due to the coupling capacitors allowing the transistor's biasing. This amplifier is reaching a higher upper frequency with a lower current consumption than the other amplifiers.

# 5 Proposed Circuits

## 5.1 Carrier Sensing Circuits

The main idea of a carrier sensing circuit is the implementation of a very simple WuRx. This WuRx is only capable of detecting a single RF pulse in order to
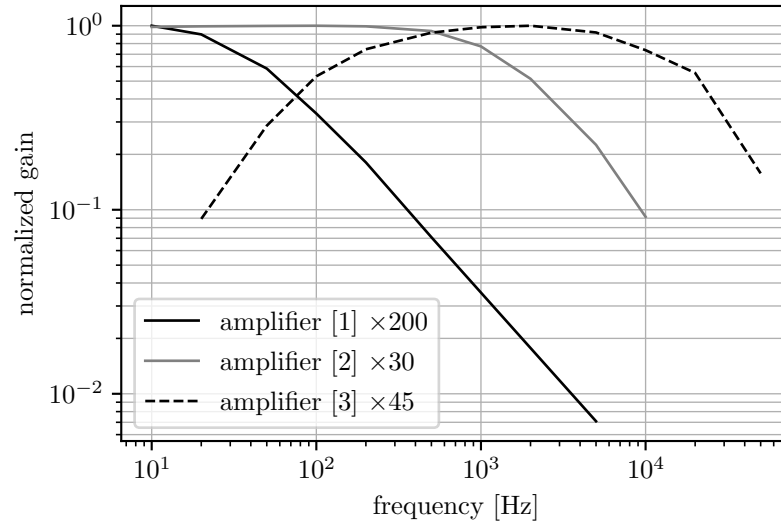
Figure 15: Measurement results of the frequency response of the three amplifier circuits

wake-up the main RF transceiver. Additional applications lie in a channel busy assessment in order to avoid transmission collisions.

### 5.1.1 Proposed Circuits

The first proposed circuit was introduced in [FSD21]. This design was further improved resulting, into a new and better implementation. The following changes were made. The biasing circuit was integrated into the first amplifier stage. The amplification factor can be reduced due to fewer losses inside the biasing circuit. This leads to the possibility to use only one amplification stage. An adaptive threshold generation is used to further reduce the current consumption. In Table 7 compares these two implementations in detail.

With the described changes, it was possible to reduce the current consumption significantly while maintaining the sensitivity at around −50 dBm. This sensitivity was measured when applying a 868 MHz RF signal with a pulse length of 5 ms. The turn-on time of the carrier sensing circuit was reduced from 450 ms to 50 ms. This was verified by an LTspice simulation. The long turn-on time of the old implementation is due to additional high-pass filter, that were needed in order to remove the additional offsets by the biasing circuit and input offsets of the OAs. The filter's time constant needed to be set accordingly in order to prevent signal distortion of the 5 ms carrier pulse.

Table 7: Comparison of carrier sensing circuits

| Parameter | Implementation [FSD21] | Improved implementation |
|---|---|---|
| Biasing circuit | Additional voltage divider with high-pass filter | Integrated into first amplifier stage |
|     Current consumption | 300 nA | 300 nA |
| LF amplifier | dual-stage non-inverting | single-stage non-inverting |
|     OA | 2× TLV521 | 1× TLV521 |
|     Total gain | 900 | 200 |
|     Current consumption | 700 nA | 350 nA |
| Comparator | TLV3691 | TLV3691 |
|     Current consumption | 75 nA | 75 nA |
| Reference generator | fixed: 100 mV | adaptive |
|     Current consumption | 300 nA | — |
| Supply voltage | 3 V | 3 V |
| Calculated supply current | 1375 nA | 725 nA |
| Measured supply current | 1400 nA | 860 nA |
| Sensitivity | −50 dBm | −51 dBm |
| Simulated turn-on time | 450 ms | 50 ms |

### 5.1.2 Usability as a Wake-up Receiver

To test the usability of the circuit as a wake-up receiver, a radio transceiver module is used. A carrier pulse at the center frequency of 868 MHz at the output power of 11 dBm is generated. Two $\lambda/2$ whip antennas are used for the transmitter and the carrier sensing test circuit. With this setup, a maximum transmission range of around 10 m can be observed [FSD21].

Interferences of other RF systems are present. Especially Wi-Fi transmitter are capable of bypassing the SAW filter due to high transmission powers. Designing a carrier sensing circuit with a sensitivity greater −50 dBm is not effective, because these interferences occur more and more frequently. Additional filtering criteria need to be introduced.

### 5.1.3 Usability as a Carrier Sensing Circuit

The second usage is found in carrier detection and collision avoidance techniques. When communicating in a wireless network, package collision is quite frequent. These collisions lead to an energy loss because the current package needs to be resent.

Modern wireless transceiver modules often have a carrier sensing circuit, clear

channel assessment module, or wake-on radio integrated. The improvement is much better sensitivity, and selectivity. But when taking a look at typical current consumption of these modes, they are in the order of 10 mA [Atm14]. The comparison of this current consumption to the current consumption of the proposed circuit shows that an improvement of factor 10.000 can be achieved [FSD21].

## 5.2 Low Frequency Correlator

### 5.2.1 Working Principle

Because of multiple RF sources in a real-life environment, the carrier sensing circuit is not sufficient to act as a reliable WuRx. With higher sensitivity false-positives occur more often. With lower sensitivity the WuPt's reception range decreases. A simple implementation to receive WuPts more reliable is to detect a special frequency inside the demodulated signal. This way, a OOK-modulated signals with a special LF signal needs to be transmitted and detected by the WuRx. For the LF correlation, the serial or universal asynchronous receiver transmitter (UART) interface of a MSP430G2553 is used. A symmetrical square-wave signal with a specific frequency can be interpreted as a valid UART signal. With the start bit being a logical 0 and stop bit a logical 1 a square wave signal results into the received hexadecimal value of 0x55. Figure 16 shows the interpretation of a square-wave signal as an UART signal. In order to match the receiver's timing constrains the bit duration $T_{bit}$ must be exactly the half of the square wave's period $T_{SW}$.
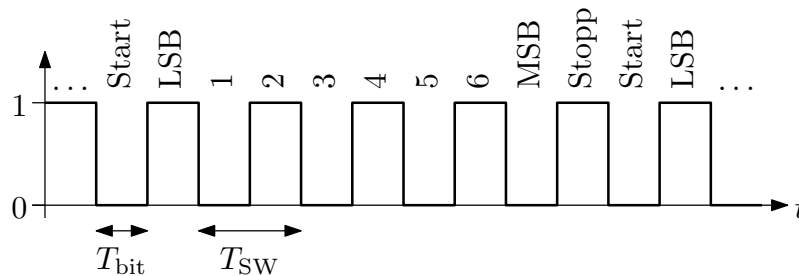


Figure 16: Interpretation of a symmetrical square-wave as a valid UART signal. $T_{bit}$ being the bit duration and $T_{SW}$ the period of the square-wave signal.

To save energy, only low-power clock sources can be used. Using a clock crystal with a frequency of 32.768 kHz leads to an MSP430's current consumption of 700 nA. It has to be noted, that running a clock crystal oscillator inside a wireless sensor node is often mandatory for timers and real-time clocks. That is why the following power consumption figures will not include the MSP430's power needs.

20

The baud rate of the UART receiver is configured by a clock divider $n$. The minimum clock divider is $n = 3$ resulting to a baud rate of 10.92 kHz and a square-wave frequency of 5.46 kHz. Due to lower frequency responses of the utilized amplifiers lower bit rates will be utilized.

### 5.2.2 Proposed Circuits

In the following section, two different implementations of a WuRx utilizing the LF correlator will be investigated. Figure 17 shows these two implementations and Table 8 lists the parameters in detail. The amplifier circuits [2] and [3] see Table 6 were used. The comparator LPV7215 was utilized due to its low current consumption and high sensitivity. The time constant of the adaptive reference generator's low-pass filter was set to $\tau = 1$ ms. The circuits' settling times were simulated with LTspice. The BJT-based implementation's settling time is significantly higher due to the amplifier circuit's coupling capacitors. Measures to decrease the settling time would either distort the signal or increase the current consumption.
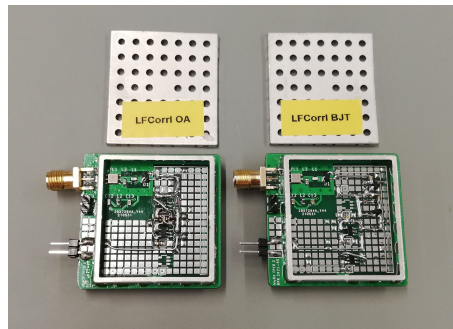


Figure 17: Photography of the two proposed circuits [2] and [3] implemented on test PCBs with WuRx RF front-end. Additional RF shielding can be applied for final sensitivity tests.

### 5.2.3 Sensitivity Measurements

The comparator output signal of the circuit is fed into the MSP430's input pin of the UART module. The UART module is configured to the specified correlation frequency. If a valid UART symbol is received by the MSP430, an interrupt is executed. If the received UART symbol is equal to 0x55, an output pin is set, signaling a successful WuPt reception. According to Figure 16 more than five OOK pulses are needed in order to receive a valid UART symbol. For the following sensitivity measurements, a WuPt is defined as 12 OOK pulses. Figure 18 shows the block diagram of the sensitivity measurement setup.

The test circuit and MSP430 are connected to the RF signal generator. A special counter circuit is build up in order to enable the RF generator to send WuPts and

Table 8: Comparison of LF correlator circuits

| Parameter | Proposed circuit [2] | Proposed Circuit [3] |
|---|---|---|
| Amplifier | OA-based [2][1] | BJT-based [3][1] |
|    Current consumption | 900 nA | 530 nA |
|    Amplification | ×30 | ×45 |
|    Cut-off frequency | ≈ 3 kHz | ≈ 10 kHz |
| Comparator [Tex16a] | LPV7215 | LPV7215 |
|    Current consumption (typ.) | 790 nA | 790 nA |
|    Propagation delay (typ.) | 13 μs | 13 μs |
| Total current consumption (calc.) | 1.69 μA | 1.32 μA |
| Total current consumption (meas.) | 1.6 μA | 1.2 μA |
| Simulated settling time | 200 μs | 30 ms |

[1] see Table 6
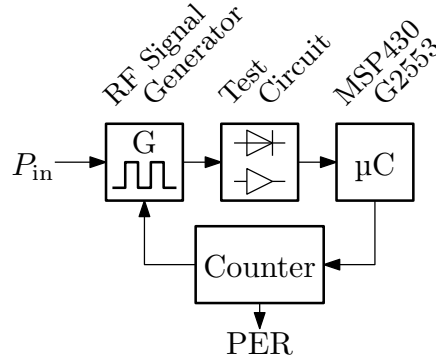


Figure 18: Block diagram of the WuRx's sensitivity measurement

count the WuPts detected by the MSP430. By comparing sent and received packet counts the packet error rate (PER) can be estimated.

Because the amplifier circuit [2] is limited to 3 kHz, a baud-rate divider of $n = 16$ was selected, resulting into a baud rate of 2048 Hz and a square-wave frequency of 1024 Hz. With 12 OOK pulses, the WuPt duration is 11.7 ms. The input power of the RF signal generator was varied in the range of −45 to −65 dBm, $N = 1000$ packets were transmitted, and the PER was estimated.

Figure 19 shows the resulting sensitivity curves of both designs. The design [2] receives the majority of the WuPts down to −55 dBm. The design [3] reaches around −60 dBm.

Because the amplifier of design [3] is capable to amplifying higher-frequency signals, a baud-rate divider of $n = 4$ with a baud-rate of 8192 Hz and a square-wave frequency of 4096 kHz was tested. With $n = 4$ the WuPt with 12 OOK pulses is only 2.93 ms. Figure 20 shows the sensitivity curves at different correlation frequencies.
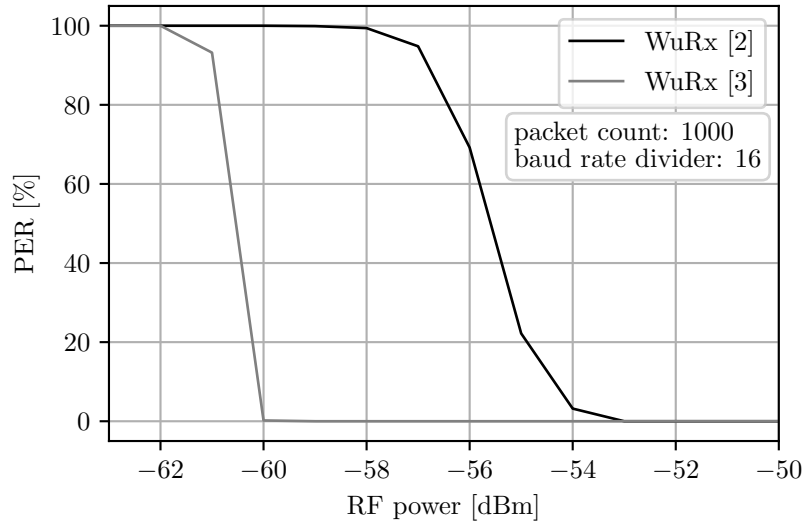
Figure 19: Packet error rate vs. input power comparing OA-based design [2] and BJT-based design [3]

Due to the higher frequency the sensitivity drops from −60 dBm to −56 dBm.
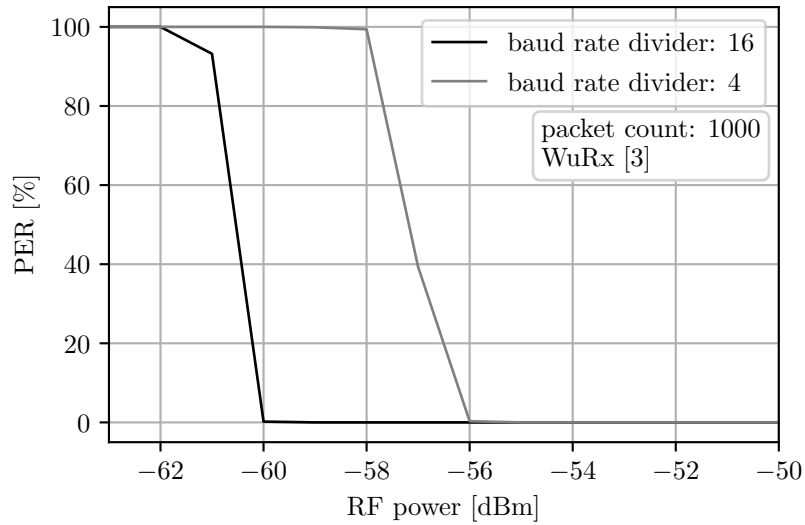


Figure 20: Packet error rate vs. input power of the BJT-based design [3] comparing slow ($n = 16$) and fast ($n = 4$) data rates

### 5.2.4 Usability as a Wake-up Receiver

To test the usability of the circuit as a WuRx, the same test procedure described in previous subsection was used. An RF transmitter with a power of 11 dBm and two λ/2 whip were used. With this setup, higher transmission ranges even through obstacles like walls could be achieved. Interferences from other RF systems could not be observed.

23

# 6 Discussion

## 6.1 Further Work

The proposed circuits show a simple way to implement WuRx without any specialized integrated circuits. The circuit's RF path is kept simple. Further investigations shall be made in order to find out, whether the theoretical values of the voltage sensitivities can be reached. The OA-based LF amplifier was optimized successfully in comparison to the publication [FSD21]. Non-inverting OA circuit with integrated biasing depletes the OA's capabilities completely while enabling a fast settling time. The comparator's adaptive threshold generation works reliable. Currently, the circuit was only built for a carrier frequency of 868 MHz. By swapping the SAW filter and matching the RF circuit other frequency bands can be used. Further tests will be made to test the circuit's performance in the 433 MHz and 2.45 GHz range. According to Friis' transmission formula [Fri46] the transmission loss of the RF signal is dependent on the wavelength resulting into higher transmission ranges when utilizing the 433 MHz band. The 2.45 GHz range is highly important due to its capability to realize high data rate transmissions.
Further work is needed to implement an address correlator in the LF correlator circuits. The microcontroller's UART module can be used to implement the data reception. Manchester encoding can be used in order to ensure a 50 % duty cycle and proper workings of the adaptive reference generator.

## 6.2 Usability as a Wake-up Receiver

The carrier sensing circuit proposed in subsection 5.1 can be used as a WuRx in shielded areas or areas with low RF activities. One application of high importance in future is a vibration measurement system inside a metal gear box. In this case only RF signals from the intended transmitter are strong enough to excite the carrier sensing circuit. The improved implementation has a faster turn-on time, lower current consumption, and a sensitivity of around −50 dBm. This circuit is suitable for the intended use case.
The LF correlator circuits are suitable for many WuRx applications. Because no WuRx addressing is implemented, all WuRx in range are excited. The OA-based implementation has lower sensitivity and higher current consumption, but faster settling time. The BJT-based implementation requires more additional components and has a slow turn-on time. With slow transmission rate WuPt of only 11.7 ms is used and with high transmission rate only 2.93 ms are needed. These WuPt duration is much faster than current implementations of [BDK18b; CAM20;

GS+20; Kaz+21].

The achieved sensitivity of around −60 dBm is a bit lower than current always-on implementations, because of an additional SAW filter enhancing the circuit's reliability, but decreasing the sensitivity by around 3 dB. Compared to [BDK18b] only general-purpose integrated circuits are used, lowering the costs, and making the search for replacement parts easy.

## 6.3 Conclusion

In this work a power-saving approach with energy detection and carrier sensing is presented. The proposed circuit utilizing the 868 MHz band was improved resulting into a sensitivity of −50 dBm, a power consumption of 2.6 µW, and a settling time of 50 ms. The maximum observed transmission range is around 10 m.

To further improve the sensitivity of this circuit, a LF correlator was added in order to differentiate wake-up packets from interferences. An implementation based on operational amplifiers and another implementation based on bipolar junction transistors was introduced. The sensitivity was increased up to −60 dBm with a power consumption of 3.6 µW. Further tests will be made in order to utilize these circuits in different frequency bands like 433 MHz or 2.45 GHz.

# References

[Agi05]     Agilent Technologies. *Agilent HSMS-285x SeriesSurface Mount Zero Bias Schottky Detector Diodes*. Datasheet. June 2005.

[ams07]     ams AG. *AS1976. AS1977 Ultra-Low Current, 1.8 V Comparators*. Datasheet. 2007.

[APM08]     Junaid Ansari, Dmitry Pankin, and Petri Mähönen. "Radio-triggered Wake-ups with Addressing Capabilities for Extremely Low Power Sensor Network Applications". In: *Int. J. Wirel. Inf. Netw.* 16 (Sept. 2008), pp. 118–130. DOI: 10.1007/s10776-009-0100-6.

[Atm14]     Atmel. *AT86RF233 - Low Power, 2.4GHz Transceiver for ZigBee, RF4CE, IEEE 802.15.4, 6LoWPAN, and ISM Applications*. 2014.

[BB03]       Inder Bahl and Prakash Bhartia. *Microwave Solid State Circuit Design*. New York: Wiley, 2003. ISBN: 978-0-471-20755-9.

[BDK18a]    Sadok Bdiri, Faouzi Derbel, and Olfa Kanoun. "A Tuned-RF Duty-Cycled Wake-Up Receiver with -90 dBm Sensitivity". In: *Sensors* 18.1 (2018). ISSN: 1424-8220. DOI: 10.3390/s18010086. URL: https://www.mdpi.com/1424-8220/18/1/86.

[BDK18b]    Sadok Bdiri, Faouzi Derbel, and Olfa Kanoun. "A wake-up receiver for online energy harvesting enabled wireless sensor networks: Technology, Components and System Design". In: De Gruyter Oldenbourg, Nov. 2018, pp. 305–320. ISBN: 9783110445053. DOI: 10.1515/9783110445053-018.

[CAM20]     Felix Cabarcas, Juan Aranda, and Diego Mendez. "OpenWuR - An Open WSN Platform for WuR-Based Application Prototyping". In: *Proceedings of the 2020 International Conference on Embedded Wireless Systems and Networks on Proceedings of the 2020 International Conference on Embedded Wireless Systems and Networks*. EWSN '20. USA: Junction Publishing, 2020, 212–217. ISBN: 9780994988645.

[CK03]       Chee-Yee Chong and S. P. Kumar. "Sensor networks: evolution, opportunities, and challenges". In: *Proceedings of the IEEE* 91.8 (2003), pp. 1247–1256. DOI: 10.1109/JPROC.2003.814918.

[Fri46]      H. T. Friis. "A Note on a Simple Transmission Formula". In: *Proceedings of the IRE* 34.5 (1946), pp. 254–256. DOI: 10.1109/JRPROC.1946.234568.

[FSD21]     Robert Fromm, Lydia Schott, and Faouzi Derbel. "An Efficient Low-power Wake-up Receiver Architecture for Power Saving for Transmitter and Receiver Communications". In: *Proceedings of the 10th International Conference on Sensor Networks - SENSORNETS*, INSTICC. SciTePress, 2021, pp. 61–68. ISBN: 978-989-758-489-3. DOI: 10.5220/0010236400610068.

[GS+20]     David Galante-Sempere et al. "Low-Power RFED Wake-Up Receiver Design for Low-Cost Wireless Sensor Network Applications". In: *Sensors* 20.22 (2020). ISSN: 1424-8220. DOI: 10.3390/s20226406. URL: https://www.mdpi.com/1424-8220/20/22/6406.

[Gam+10]    G. U. Gamm et al. "Low power wake-up receiver for wireless sensor nodes". In: *2010 Sixth International Conference on Intelligent Sensors,*

*Sensor Networks and Information Processing*. 2010, pp. 121–126. DOI: 10.1109/ISSNIP.2010.5706778.

[Kaz+21]     Giannis Kazdaridis et al. *eWake: A Novel Architecture for Semi-Active Wake-Up Radios Attaining Ultra-High Sensitivity at Extremely-Low Consumption*. 2021. arXiv: 2103.15969 [cs.AR].

[Mag+16]     M. Magno et al. "Design, Implementation, and Performance Evaluation of a Flexible Low-Latency Nanowatt Wake-Up Radio Receiver". In: *IEEE Transactions on Industrial Informatics* 12.2 (2016), pp. 633–644. DOI: 10.1109/TII.2016.2524982.

[Mic19]      Microchip. *MCP6141/2/3/4 - 600 nA, Non-Unity Gain Rail-to-Rail Input/Output Op Amps*. Datasheet. 2019.

[Piy+17]     Rajeev Piyare et al. "Ultra Low Power Wake-Up Radios: A Hardware and Networking Survey". In: *IEEE Communications Surveys & Tutorials* PP (June 2017). DOI: 10.1109/COMST.2017.2728092.

[RF319]      RF360 Europe GmbH. *SAW RF filter - B39871B3725U410*. Datasheet. 2019.

[Sky08]      SkyWorks Inc. *Mixer and Detector Diodes*. Aug. 2008. URL: https://www.skyworksinc.com/search?q=200826a.

[Sky18]      Skyworks Solutions, Inc. *Surface-Mount Mixer and Detector Schottky Diodes*. Datasheet. June 2018.

[STM13]      STMicroelectronics NV. *TS881 - Rail-to-rail 0.9 V nanopower comparator*. Datasheet. Dec. 2013.

[Tex01]      Texas Instruments. *Single-Supply Op Amp Design Techniques*. Application Report. Mar. 2001.

[Tex15]      Texas Instruments. *TLV3691 0.9-V to 6.5-V, Nanopower Comparator*. Datasheet. Nov. 2015.

[Tex16a]     Texas Instruments. *LPV7215 Micropower, CMOS Input, RRIO, 1.8-V, Push-Pull Output Comparator*. Datasheet. Aug. 2016.

[Tex16b]     Texas Instruments. *TLV521 NanoPower, 350nA, RRIO, CMOS Input, Operational Amplifier*. Datasheet. May 2016.

[TCP17]      Le-Giang Tran, Hyouk-Kyu Cha, and Woo-Tae Park. "RF power harvesting: a review on designing methodologies and applications". In: *Micro and Nano Systems Letters* 5.1 (Feb. 2017). DOI: 10.1186/s40486-017-0051-0.